

Kinetic analysis of ultrasound leaching of nickel laterite ore

P. Paunović*, G. Načevski, A. Petrovski, A. Tomova, A. Grozdanov, A. T. Dimitrov

*Faculty of Technology and Metallurgy, University “Sts. Cyril and Methodius”
Ruger Bošković Str., 16, 1000 Skopje, R. Macedonia*

Received October 30, 2018; Revised January 10, 2019

The subject of this study is the ultrasound leaching process of nickel-bearing laterite ore from Ržanovo, R. Macedonia. The studied ore was characterized by means of X-ray fluorescence method (XRF), X-ray diffraction method (XRD), thermal analysis (TGA, DTA, DTG) and optical microscopy. The influence of sulfuric acid concentration (1, 2 and 3 M H₂SO₄) on the extracted Ni (% wt.) was investigated. Further, ultrasound leaching at different temperatures (298, 313, 323 and 348 K) was performed. These results were used for kinetic analysis of the process. It was found that for 3 M H₂SO₄, the best fitting has shown the Ginstling-Braunshtein model, which points out that the limiting step of the process is diffusion. Activation energy was calculated to be 33.1 kJ·mol⁻¹, which confirms the diffusion controlled process.

Keywords: nickel-bearing laterite ore, ore characterization, ultrasonic leaching, kinetic models, activation energy.

INTRODUCTION

Nickel and its alloys have important role in modern life for variety of applications [1]. Industrial production of nickel is based on sulfide and laterite (oxide) ores. Although laterite ores are more abundant (about 70 % of the land reserves), with lower negative impact to environment and lower mining cost, their contribution in the world's nickel production is only 40 % [2-4]. The present technological processes for nickel production from laterite ores are based on both pyro- and hydrometallurgical routes [5, 6]. The pyrometallurgical ones include ferronickel smelting *via* the rotary kiln-electric furnace (RKEF) process and nickel matte smelting, while the hydrometallurgical techniques include high-pressure acid leaching (HPAL) and the Caron process. HPAL procedure requires expensive aggregates – autoclaves, while in the Caron process, pyrometallurgical reduction roasting is included before the ammonia leaching.

In finding new cheaper and ecologically friendly technologies for nickel extraction from laterite ores, the research work was focused on development of leaching under atmospheric pressure or atmospheric leaching, AL. The research studies of AL are directed to the use of different acid solvents such as sulfuric acid [7], hydrochloric acid [8], nitric acid [9], citric acid, acetic acid and oxalic acid [10,11]. With an appropriate optimization of the AL process, i.e. with overcoming the usual problems such as high acid consumption, high content of iron content in the solution and high residual acid concentration, AL could reach the effectiveness of

HPAL process [12].

The aim of this work was to investigate the LA process using sulfuric acid, intensified by ultrasound. Also, kinetic analysis of the ultrasound atmospheric leaching was done, determining both, the rate-limiting step and the activation energy of the leaching process.

EXPERIMENTAL

Ore

The subject of study was low-grade nickel-bearing laterite ore from Ržanovo mining area near the ferronickel smelting plant FENI INDUSTRI, Kavadarci in R. Macedonia. It belongs to intermediate type Saprolitic ores classified in the class C, due to increased content of MgO (12–16 %, wt.) and Fe (25–33 %, wt.). Mechanical preparation of the ore was performed within the production line of the FENI INDUSTRI, Kavadarci. The set of different sieves (0.200 mm, 0.104 mm, 0.074 mm, 0.043 mm and 0.037 mm) was used for determination of the granulometric composition. The dominant fraction with the highest content of Ni was chosen for further study. Before the leaching, magnetic separation was done in order to reduce the amount of Fe, and to increase the Ni content.

The composition of the ore was measured by X-ray fluorescence spectroscopy, using XRF ARL 9900 spectrometer. Thermal analysis was performed by TGA/DTA/DTG technique, using Perkin Elmer Diamond instrumentation. The sample was heated from 25 to 1000 °C, with a heating rate of 20 °C·min⁻¹. XRD measurements were carried out by X-ray powder diffractometer

* To whom all correspondence should be sent.

Philips APD 15, with CuK α radiation. The diffraction data were collected at a constant rate of 0.02 deg \cdot s $^{-1}$ over an angle range of 2θ from 5 deg to 80 deg. Microscopic observation of the ore morphology was performed by Jeol Superprobe 737 microscope.

Ultrasonic leaching

Experimental setup for ultrasonic leaching of Ni-bearing ore is shown in Fig. 1. Glass reactor (1) is immersed into ultrasound bath (2) filled with water. The ultrasound bath has a system for temperature regulation. The aqueous cooler (3) connected with a tap through rubber hose (4) provides cooling of the reactor and avoiding evaporation of the solvent, thereby increasing the pressure in the reactor. The temperature is measured with a mercury thermometer (5).



Figure 1. Experimental setup for ultrasound leaching.

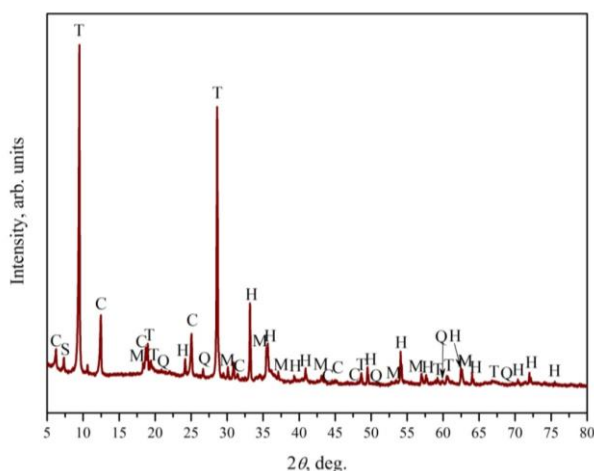


Figure 2. XRD spectrum of the Ržanovo's ore: H - hematite (Fe $_2$ O $_3$, rhombohedral), C - clinocllore ((Mg $_5$ Al)(Al,Si) $_4$ O $_{10}$ (OH) $_8$, triclinic), T - talc (Mg $_3$ Si $_4$ O $_{10}$ (OH) $_2$, monoclinic), Q - quartz (SiO $_2$, hexagonal), S - stilpnomelane (Fe $_2$ (Si $_3$ O $_9$), triclinic), M - magnetite (Fe $_3$ O $_4$, cubic).

As a solvent, H $_2$ SO $_4$ with different concentrations (1, 2 and 3M) was used. The ratio of solid vs. liquid phase was 1:50 (5g ore in 250 ml aqueous solution of H $_2$ SO $_4$). The leaching was performed under atmospheric pressure at different temperatures: 25, 40, 50 and 75 °C (298, 313, 323 and 348 K). For each leaching experiment, samples of 5 ml were taken at the following time interval: 5, 15, 30, 60, 90, 120 and 150 min.

Concentration of leached Ni was determined by atomic absorption spectrometry (AAS) using a spectrometer model PinAAcle 900F (PINAACLE900F).

RESULTS AND DISCUSSION

Preparation and characterization of ore

Chemical composition of the raw ore is shown in Table 1. It can be seen that Ržanovo's ore belongs to the low-grade nickeliferrous laterite ores with Ni content of 0.85 %, wt., moderate content of Fe (27.7 %, wt.) and increased content of magnesia (14.3 %, wt.) and silica (32.3 %, wt.). Present minerals within the studied lateritic ore were detected by XRD analysis, the corresponding spectrum is shown in Figure 2. According to the XRD spectrum, dominant mineral is hematite (Fe $_2$ O $_3$), while less, but considerable amount have shown talc (Mg $_3$ Si $_4$ O $_{10}$ (OH) $_2$) and clinocllore ((Mg $_5$ Al)(Al,Si) $_4$ O $_{10}$ (OH) $_8$). Quartz (SiO $_2$), magnetite (Fe $_3$ O $_4$) and stilpnomelane (Fe $_2$ (Si $_3$ O $_9$)) are shown as minor phases.

After mechanical preparation (crushing and milling), the granulometric composition was determined by sieve analysis. Corresponding composition of different granulometric fractions and corresponding distribution of the ore's components within each fraction is shown in Table 2. The finest fraction (below 0.037 mm) has shown to be the dominant one (67.2%), containing increased amount of Ni (up to 0.92%) and it was selected for further treatment. Before the leaching, magnetic separation was performed in order to reduce the amount of Fe. Ni mostly remains in the non-magnetic fraction, while Fe turns to magnetic one. As can be seen in Table 3, non-magnetic fraction contains a considerably decreased amount of Fe, up to 16.76 %, while the Ni content increased to 1.03%. This fraction was further submitted to the leaching study.

The results of thermal analysis of the ore are shown in Fig. 3. The first DTG maximum is less pronounced and appears at 85 °C. It is followed by low weight loss of 0.15 % (TG curve) and corresponds to removal of the physically adsorbed moisture of the previously dried ore.

Table 1. Composition of raw Ržanovo's ore

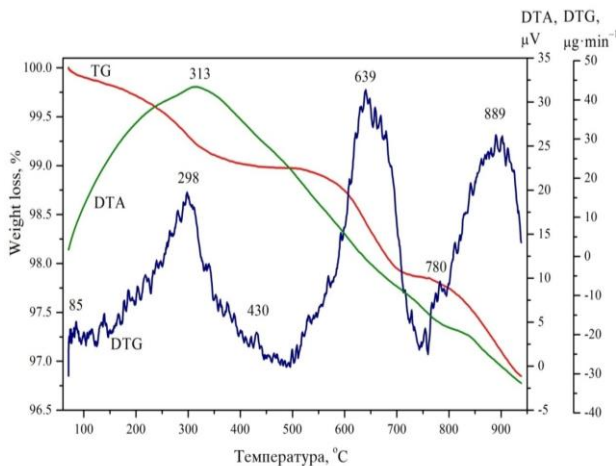
Components	Fe	Ni	Co	Cr	CaO	MgO	Al ₂ O ₃	SiO ₂
% wt.	27.70	0.85	0.04	1.90	1.70	14.30	1.50	32.30

Table 2. Granulometric composition after mechanical preparation of the ore

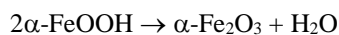
Granulometric fraction, mm	Granulometric composition, % wt.	Contribution of the components in each fraction, % wt.							
		Fe	Ni	Co	Cr	CaO	MgO	Al ₂ O ₃	SiO ₂
-0.200 + 0.104	11.5	33.09	0.75	0.04	2.0	1.7	13.1	1.4	25.6
-0.104 + 0.074	11.0	34.28	0.75	0.04	1.9	1.6	12.9	1.4	23.9
-0.074 + 0.043	7.3	32.59	0.8	0.04	1.9	1.8	13.1	1.6	25.4
-0.043 + 0.037	3.0	30.00	0.85	0.04	1.9	1.8	13.2	1.5	27.2
-0.037	67.2	24.75	0.92	0.04	1.9	1.7	14.7	1.6	35.8

Table 3. Composition after magnetic separation of the ore fraction -0.037 mm

Fraction	Contribution, % wt.	Fe	Ni	CaO	MgO	SiO ₂
Magnetic	5.70	48.11	0.35	1.14	10.55	9.25
Non-magnetic	94.30	16.76	1.04	1.73	15.26	44.26

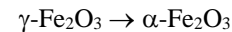
**Figure 3.** TGA-DTA-DTG spectra of the Ržanovo's ore.

The next DTG maximum at 297 °C is followed with weight loss of near 1 % and corresponds to removal of hydroxylic water (dehydration). It is likely that the hydroxylic water in the ore is present in the goethite, α -FeOOH, and this peak corresponds to the transformation of the goethite to hematite by the releasing of hydroxylic water [13,14]:



The relatively low temperature of this transformation indicates that the hematite is amorphous or is poorly crystalline with a very small size of crystalline grains [13,15]. This is a logical explanation why the goethite was not detected by the XRD analysis. According to the literature, a highly crystalline goethite transforms at 385 °C, showing strongly shaped peak [16,17]. Also, the dehydration occurs directly without the

formation of intermediary phases [18], or a small amount of magnetite can appear as an intermediate [19]. Also, during the transformation, there may be a significant change in the porosity and morphology of the ore particles [20]. Less pronounced DTG maximum is recorded at 430 °C. This maximum can be attributed to the partial transformation of the maghemite (γ -FeOOH) to hematite:



Maghemite was previously detected by XRD analysis. At 640 °C a more pronounced DTG peak is positioned, followed by a loss of mass of about 2%. This peak corresponds to a complete transformation of the maghemite to hematite [21]. A less intense peak was recorded at 720 °C [13], with a small additional weight of 0.3% (total 2.3%). According to the literature, in this temperature range there is increased mobility of the atoms, which leads to an increase of activation energy, to loss of the anisotropy of the oblique of the hematite grains and to interstitial sintering which means beginning of agglomeration of the grains, and further reduction of the real surface of the material. The DTG peak appearing at 890 °C corresponds to transformations in nickel-iron serpentines [22].

Microscopic images of the ore morphology are shown in Fig. 4. In Fig. 4a one can see a matrix of clay-based minerals intimately mixed with iron oxides formed by erosion. In some cases, small polygonal grains of corroded magnetite with gray color and good reflection ability are observed (Fig. 4b).

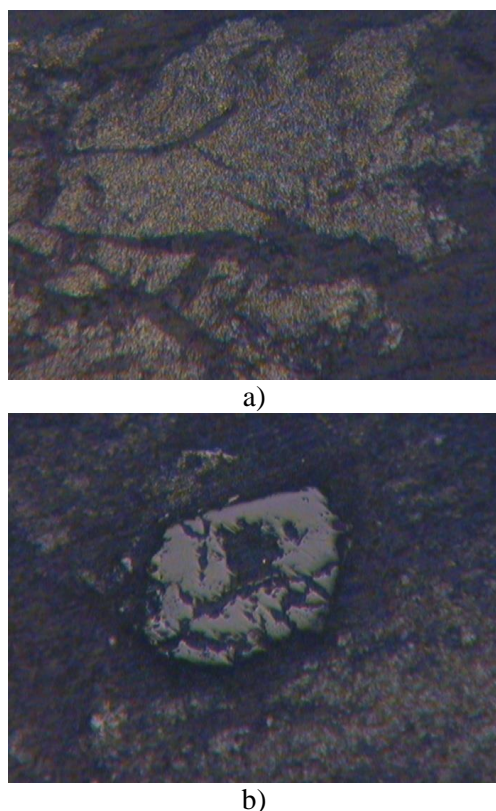


Figure 4. Microscopic images of the Ržanovo's ore.

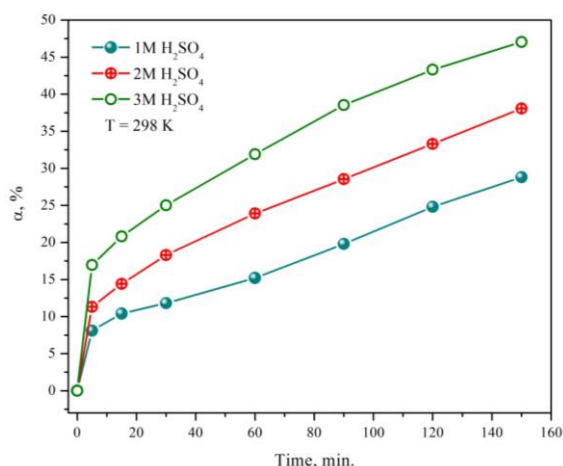


Figure 5. Diagram of yield of leached fraction α – time dependence for different concentrations of H_2SO_4 at ambient temperature.

Ultrasound leaching

The first step in the study of the ultrasound leaching of nickel laterite ore was the determination of the influence of solvent (H_2SO_4) concentration at ambient temperature (298 K). In Fig. 5 is shown the change of the yield of the leached fraction (α) during the leaching process. As can be seen, the yield of the leached fraction increases with time. Within the experimental time, the diffusion region of the curve is not reached. Also, with increasing of the solvent (H_2SO_4) concentration, the yield of the leached fraction increased, from 28.8 % in 1M H_2SO_4 , to 47.06 % in 3M H_2SO_4 .

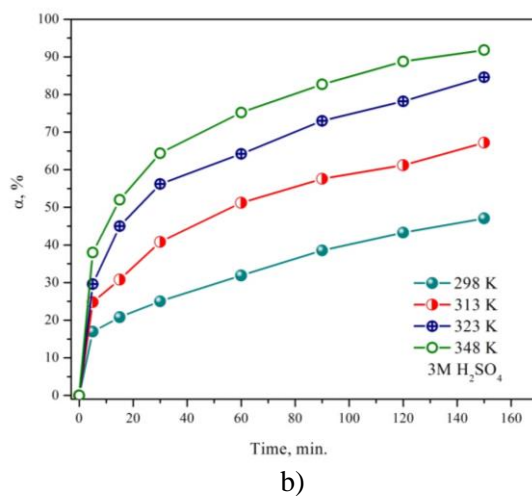
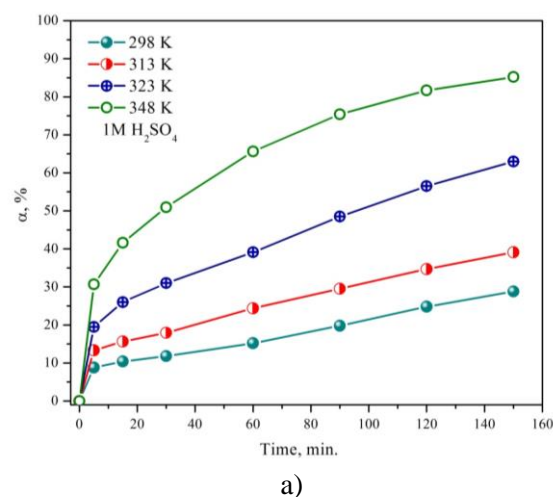


Figure 6. Diagram of yield of leached fraction α – time dependence for different temperatures in a) 1 M H_2SO_4 and b) 3 M H_2SO_4 .

In Fig. 6, the change of the yield of the leached fraction at different temperatures is shown, for 1 and 3 M H_2SO_4 . It is obvious that the temperature considerably intensifies the leaching process. After 150 min leaching in 1 H_2SO_4 , the yield of the leached fraction increased from 28.8 % at ambient temperature (298 K) to 85.2 % at 75 °C (348 K). In 3 M H_2SO_4 , the rise of α ranged from 47.06 % at ambient temperature (298 K) to even 91.8 % at 75 °C (348 K). In Table 4, the comparison of the yield of leached fraction of ultrasound leaching and leaching with magnetic stirrer [23] after 120 min at 75 °C (348 K) is given. As can be seen, the ultrasound considerably increases the leaching process. In 3 M H_2SO_4 , the maximal yield of the leached fraction is 70.3 %, while in 1 M H_2SO_4 with ultrasound leaching this yield is 81.68 %, by almost 10 % higher. In 3 M H_2SO_4 with ultrasound leaching the yield of the leached fraction is 88.8 %, almost 20 % higher. Under the action of ultrasound, ultrasonic flows and cavitation occur in the solution, where the fluid intensively mixes and penetrates into the pores and cracks of the ore

particles. At more intense ultrasound regimes, one can come to cavitation destruction of solid particles and surface films. This increases the reaction surface of the solid ore particles, decreases the diffusion layer, and all this contributes to considerable intensifying the leaching process.

Table 4. The yield of leached fraction α (%), obtained at different leaching regimes after 120 min at 75 °C (348 K)

	Leaching regimes		
	Magnetic stirrer 3 M H ₂ SO ₄	Ultrasound 1 M H ₂ SO ₄	Ultrasound 3 M H ₂ SO ₄
α , %	70.32	81.68	88.8

Kinetic analysis of the ultrasound leaching

In general, leaching of nickel laterite ores can be described by the shrinking core model (Fig. 7), where the chemical reaction on the core surface or diffusion can be rate-determining step of the process [24,25].

If the leaching process is controlled by a chemical reaction, it can be described by the Spenser-Topley-Kewan model [26]:

$$1 - (1 - \alpha)^{\frac{1}{3}} = k_s \cdot t, \tag{1}$$

$$k_s = \frac{k \cdot C}{r_0 \cdot \rho}, \tag{2}$$

where α is yield of reacted fraction, k_s is Spenser-Topley-Kewan rate constant, k reaction rate constant, C is concentration of the solid reactant (ore particle), r_0 is radius of the solid reactant, ρ is density of the solid reactant and t is duration of the chemical reaction.

If the leaching process is controlled by the diffusion, it can be described by the Ginstling-Braunshstein model [27]:

$$1 - \frac{2}{3} \cdot \alpha - (1 - \alpha)^{\frac{2}{3}} = k_G \cdot t \tag{3}$$

$$k_G = \frac{2 \cdot M \cdot D \cdot C}{a \cdot \rho \cdot r_0^2} \tag{4}$$

where k_G is Ginstling-Braunshstein rate constant, M is molecular weight of the solid reactant, D is diffusion coefficient and a is a stoichiometric coefficient.

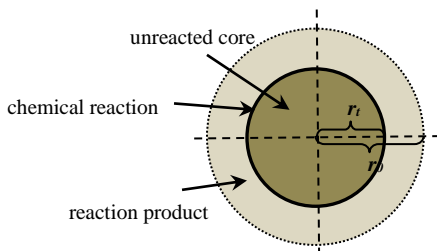


Figure 7. Schematic view of the shrinking core model: r_0 - starting radius of the reacting ore article; r_1 -

radius of the reacting ore article after some time t .

The data from the diagrams in Figs. 8 and 9 were replaced in the model equations (1) and (3), and the corresponding straight-lines are shown in Figs. 10 and 11 for 1 and 3 M H₂SO₄, respectively. The leaching process in 1 M H₂SO₄, at lower temperatures (from 25 to 50 °C) was described by the Spenser-Topley-Kewan equation, which means that in this temperature region the rate-determining step of the process is the chemical reaction. At higher temperatures, Ginstling-Braunshstein model describes the process better and the rate-determining step of the process is diffusion. The leaching process in 3 M H₂SO₄ in the whole temperature region is better described by the Ginstling-Braunshstein model. This points out diffusion as rate-determining step of the ultrasound leaching process.

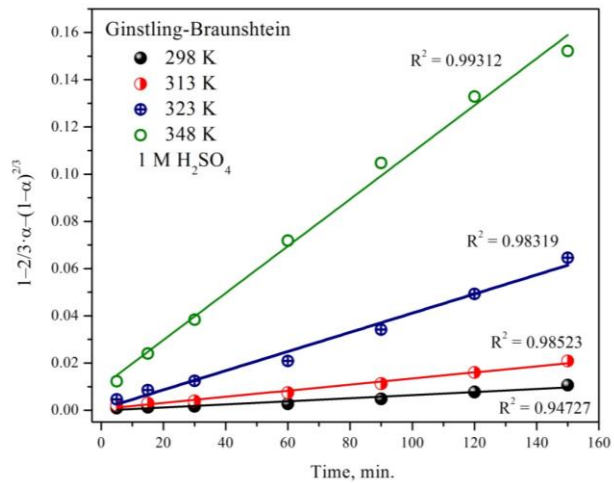
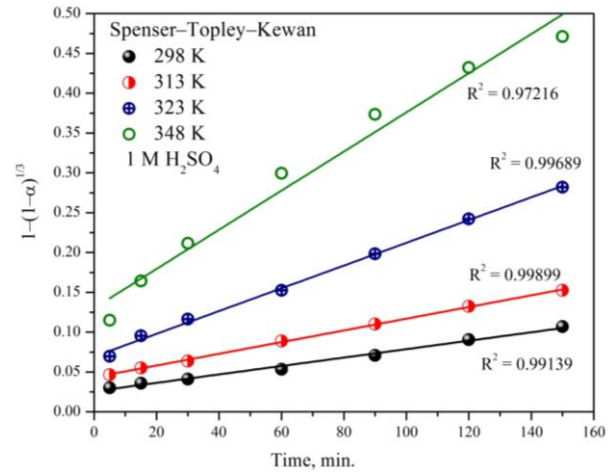
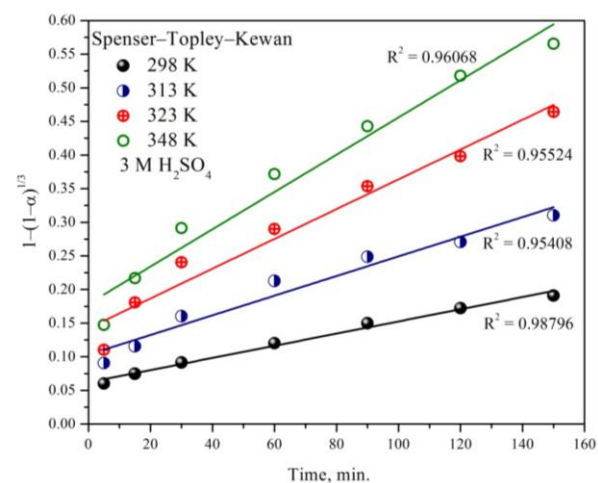
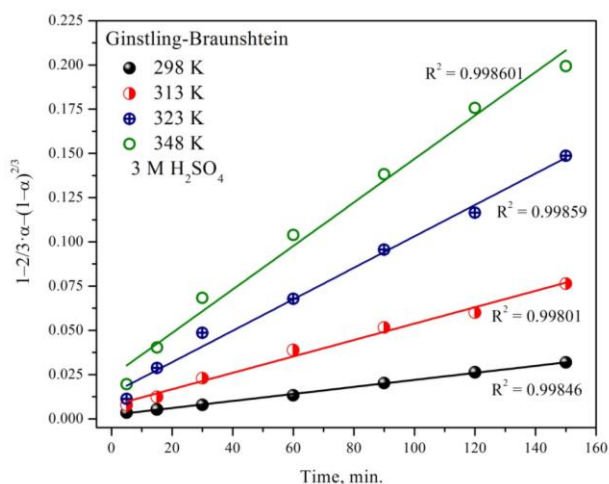


Figure 8. Linear fit of nickel leaching process in 1 M H₂SO₄ described by a) Spenser-Topley-Kewan model and b) Ginstling-Braunshstein model.



(a)



(b)

Figure 9. Linear fit of nickel leaching process in 3 M H₂SO₄ described by a) Spenser-Topley-Kewan model and b) Ginstling-Braunshtein model.

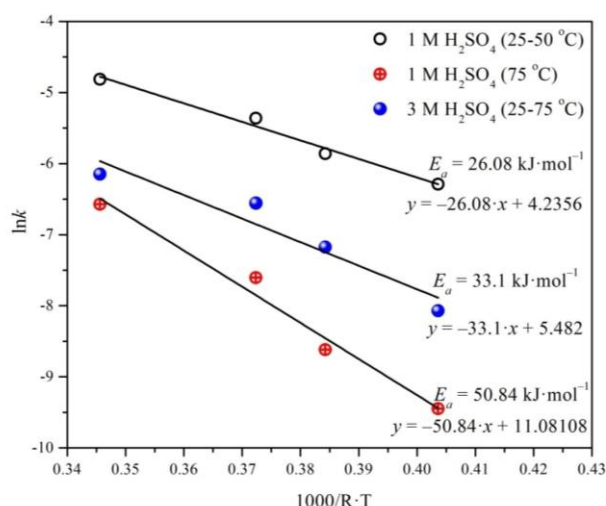


Figure 10. Arrhenius plots of nickel leaching process.

Using the Arrhenius equation:

$$\ln k = -\frac{E_a}{R \cdot T} + \ln A \quad (5)$$

where k can be Spenser-Topley-Kewan (k_S) or Ginstling-Braunshtein (k_G) rate constant, R is universal gas constant, T is temperature and A is the Arrhenius constant, the activation energy, E_a of the leaching process can be determined by further derivation of the previous experimental data and results. In Fig. 10, constructed straight-lines of Arrhenius equation and determined values of activation energy for the leaching process are shown. At lower temperature range to 50 °C in 1 M H₂SO₄, activation energy was determined using the temperature dependence of the Spenser-Topley-Kewan rate constant (k_S) and showed a value of 26.08 kJ·mol⁻¹·K⁻¹. Corresponding value of E_a for higher temperature region, determined using temperature dependence of the Ginstling-Braunshtein rate constant (k_G), is 50.84 kJ·mol⁻¹·K⁻¹. These values are in agreement with the literature data. Activation energy for leaching process in 3 M H₂SO₄, using k_G , in whole temperature region was determined to be 33.1 kJ·mol⁻¹·K⁻¹.

CONCLUSIONS

According to the above presented results, we can draw the following conclusions:

1. Ržanovo's ore belongs to the low-grade nickel-ferrous laterite ores with low Ni content of 0.85 %, wt., moderate content of Fe (27.7 %, wt.) and increased content of magnesia (14.3 %, wt.) and silica (32.3 %, wt.). Dominant compound in the ore is hematite, α-Fe₂O₃, but there is also a considerable amount of talc, Mg₃Si₄O₁₀(OH)₂ and clinochlor, (Mg₅Al)(SiAl)₄O₁₀(OH)₈ and less of quartz, SiO₂, magnetite, Fe₃O₄, maghemite, γ-Fe₂O₃ and stilpnomelan, Fe₂(Si₃O₉).

2. According to granulometric analysis, the richest fraction with Ni (0.92 %, wt.) is -0,037 mm. After magnetic separation, the content of Ni in the non-magnetic fraction increases to 1.03%.

3. Maximal nickel extraction of 91.8 % was achieved by ultrasound leaching in 3M H₂SO₄ at 75 °C.

4. Ultrasound significantly intensifies the leaching process compared to the magnetic stirrer. Ultrasound causes ultrasonic flows and cavitation in the solution, where the fluid intensively mixes and penetrates into the pores and cracks the ore particles. As a result, there is an increase of the reaction surface of the solid ore particles, decrease of the diffusion layer, contributing to considerable intensifying the leaching process.

5. The leaching process in 1M H₂SO₄ at lower temperatures is best described by the Spenser-Topley-Kewan model (chemically controlled), while at higher temperatures - by the Ginstling-Braunshstein model (diffusion controlled). The leaching process in 3 M H₂SO₄ in the whole experimental temperature region is best described by the Ginstling-Braunshstein model (diffusion controlled). Activation energy for the leaching in 1M H₂SO₄ was determined to be 26.08 kJ·mol⁻¹·K⁻¹ for chemically controlled and 50.84 kJ·mol⁻¹·K⁻¹ for diffusion controlled process. Activation energy in 3 M H₂SO₄ was determined to be 33.1 kJ·mol⁻¹·K⁻¹ in the whole temperature region.

REFERENCES

1. F. Crundwell, M. Moats, V. Ramachandran, T. Robinson, W.G. Davenport, Extractive Metallurgy of Nickel, Cobalt and Platinum Group Metals, Elsevier, 2011.
2. A. D. Dalvi, W. Gordon Bacon, R. C. Osborne, The Past and the Future of Nickel Laterites, PDAC 2004 International Convention, Trade Show & Investors, Exchange, Toronto, March 7-10, 2004.
3. N. D. H. Munroe, *Metallurgical and Materials Transactions B*, **28**, 995 (1997).
4. USGS Bureau of Mines Yearly Statistics 1950-2003.
5. E. Ozberk, A. S. Gendron, G. H. Kaiura, Review of Nickel Smelters, Proceedings- Nickel Metallurgy, Vol. I: Extraction and Refining of Nickel, E. Ozberk and S. W. Marcuson (eds.), Met Soc. CIM and NiDI, Montreal (1986), p. 304.
6. S. R. Stopić, B. G. Friedrich, *Military Technical Courier*, **64**, 1033 (2016).
7. R.G. McDonald, B.I. Whittington, *Hydrometallurgy*, **91**, 35 (2008).
8. R.G. McDonald, B.I. Whittington, *Hydrometallurgy*, **91**, 56 (2008).
9. B. Ma, C. Wang, W. Yang, B. Yang, Y. Zhang, *Miner. Eng.*, **45** 151 (2013).
10. S. Sahu, N. C. Kavuri, M. Kundu, *Braz. J. Chem. Eng.*, **28**, 251 (2011).
11. A. Pawlowska, Z. Sadowski, *Physicochem. Probl. Miner. Process.*, **53**, 869 (2017).
12. E. Büyükakinci, Y.A. Topkaya, *Hidrometallurgy*, **97**, 33 (2009).
13. F. A. López, M. C. Ramirez, J. A. Pons, A. López-Delgado, F. J. Alguacil, *J. Therm. Anal. Calorim.*, **94**, 517 (2008).
14. Y.V. Swamy, B.B. Kar, J.K. Mohanty, *Hydrometallurgy*, **69**, 89 (2003).
15. H. Liu, T. Chen, X. Zou, C. Qing, R. L. Frost, Thermal treatment of natural goethite: Thermal transformation and physical properties, *Thermochim. Acta*, **568**, 115 (2013).
16. R. Derie, D. M. Ghodsi, C. Calvo-Roche, *J. Therm. Anal. Calorim.*, **9**, 435 (1976).
17. U. Schwertmann, *Thermochim. Acta*, **78**, 39 (1984).
18. C. J. Goss, *Mineral. Mag.*, **51**, 437 (1987).
19. Ö. Özdemir, D. J. Dunlop, *Earth Planet. Sci. Lett.*, **177**, 59 (2000).
20. V. Balek, V. J. Šubr, *Pure Appl. Chem.*, **67** 1839 (1995).
21. X. Song, J-F. Boily, *J. Phys. Chem. A*, **120**, 6249 (2016).
22. S. Stopić, B. Friedrich, R. Fuchs, *Erzmetall*, **56**, 198 (2003).
23. G. Načevski, P. Paunović, A. Petrovski, A. Grozdanov and A. T. Dimitrov, Leaching of nickel from Ržanovo's lateritic ore, Book of Abstracts, 3rd Metallurgical & Materials Engineering Congress of South-East Europe, MME SEE 2017, Belgrade, 1-3 June, 2017, p. 53.
24. O. Levenspiel, Chemical Reaction Engineering, John Wiley & Sons, Inc., New York, 1999.
25. F. Habashi (ed.), Handbook of extractive metallurgy, Volume I, WILEY-VCH, Weinheim, 1997.
26. W. D. Spenser, B. Topley, *J. Chem. Soc.*, **27**, 2633 (1929).
27. A. M. Ginstling, B. I. Braunshstein, *J. Appl. Chem. USSR*, **23**, 1327 (1950).